

rings A (Fig. 2) and B, at the edges of the eccentric ring ($\approx 1.446 R_S$), near all gaps within the Cassini division and ring A, and even at ring F. No diffraction is observed at the interface between rings B and C or between the interior of ring A and the bright outer band of the Cassini division discovered by Pioneer 11 at $\approx 2.01 R_S$. This variation in the character of the edges may reflect variations in the underlying mechanisms responsible for their formation. However, the fact that features exhibiting edge diffraction occur over the inner and outer parts of the rings suggests a common causal process throughout the ring system.

On the basis of the wavelength employed, these results apply to particles in the rings with diameters greater than about 1 cm. Particles substantially smaller than 1 cm are in the Rayleigh scattering regime at $\lambda = 3.6$ cm and are probably of little importance in the intensity measurements considered here (8).

Estimates of the edge thickness based on ring occultation of the star δ -Scorpii were reported by the Voyager photopolarimeter experiment team (9). The characteristic bound obtained was about 125 m, which is consistent with the bounds reported here. These results complement one another in that they apply to different ranges in the particle size distribution. Optical extinction measurements apply to the collection of particles larger than about 2×10^{-7} m, whereas the radio results apply to the collection of particles larger than about 1×10^{-2} m. Since the stellar and radio occultations were obtained at different times and different geometries, they do not necessarily refer to the same characteristic of the edge. For example, a thin sheet of small particles could extend beyond the edge defined by the radio occultation, yielding the same thickness results for the two experiments, but without coincidence between the location of the discontinuity at optical and microwave wavelengths.

The radio occultation data also contain information on the variations of the phase of the complex coherent signal whose intensity was used to compute the diffraction patterns presented above. In effect, the coherent data correspond to a one-dimensional sampling of the microwave hologram formed behind the rings. By use of an inverse Fresnel transform it may be possible to obtain a more precise measure of edge characteristics than can be inferred by modeling.

ESSAM A. MAROUF
G. LEONARD TYLER

Center for Radar Astronomy,
Stanford University,
Stanford, California 94305

References and Notes

1. The Voyager radio science ring occultation experiment is described by V. R. Eshleman, G. L. Tyler, J. D. Anderson, G. Fjeldbo, G. S. Levy, G. E. Wood, and T. A. Croft [*Space Sci. Rev.* 21, 207 (1977)]; preliminary results are given by G. L. Tyler, V. R. Eshleman, J. D. Anderson, G. S. Levy, G. F. Lindal, G. E. Wood, and T. A. Croft [*Science* 212, 201 (1981)].
 2. The theory of radio occultation by planetary rings is given by E. A. Marouf, G. L. Tyler, and V. R. Eshleman [*Icarus* 49, 161 (1982)].
 3. Waves propagating through the rings can be separated into coherent and incoherent components, corresponding to deterministic or random behavior of the signal phase. The coherent and incoherent waves correspond to the direct (or reduced) and scattered (or diffuse) waves of radiative transfer theory [S. Chandrasekhar, *Radiative Transfer* (Dover, New York, 1960)]. We use the term coherent to emphasize the monochromatic nature of the experiment, which is not usually important in related optical scattering observations. Experimentally, the two components were readily distinguished on the basis of differential Doppler effects. The coherent wave was essentially unchanged in frequency from the value expected on the basis of the spacecraft motion with respect to the earth receiving station. Scattered signals, however, generally undergo an additional Doppler shift as a result of interaction with moving particles that are not along the geometric line of sight. This separation of components for radio occultations by rings is discussed in E. A. Marouf, thesis, Stanford University (1975) and in (2).
 4. The rings are assumed to consist of a many-particle-thick differentially rotating slab of material that can be described in terms of average loss and scattering coefficients per unit volume. For this assumption, the minimum thickness must be many wavelengths. Estimates of the volumetric packing of the rings are in the range 10^{-3} to 10^{-2} [M. S. Bobrov, in *Surfaces and Interiors of Planets and Satellites*, A. Dollfus, Ed. (Academic Press, New York, 1970), pp. 377-458] and are consistent with this model.
 5. The Voyager imaging team reported at least two narrow irregular ringlets within the Encke gap [B. A. Smith *et al.*, *Science* 215, 504 (1982)].
- These ringlets could also produce coherent diffraction, which would perturb the overall pattern formed by the edges acting alone.
6. An oblique ray that enters or exits the ring through a blunt edge will not experience the full opacity of the slab. This will cause the transition from the opacity of the slab to that of free space to occur over a finite transition width W , causing the edge to appear less sharp. The width W depends on the inclination angle ξ of the line of sight to the ring plane and the angle Ψ between the edge and the projection of the line of sight on the ring plane. An upper bound on slab thickness T in the vicinity of the edge is then $T \leq W \tan \xi / \cos \Psi$. The results reported here correspond to $\Psi \approx 36^\circ$ and $\xi \approx 5.9^\circ$.
 7. Ring B is excluded from this list. Typical values for the oblique microwave opacity in ring B exceed $\tau \sim 10$. We cannot obtain the necessary time resolution to observe diffraction from ring B features at the much lower signal-to-noise ratios obtained for ring B. Adequate signal-to-noise ratios would be achieved for a similar experiment at larger ring openings.
 8. The importance of the small particles depends on the size distribution. Particles more than about 1 cm in diameter remove energy from the $\lambda = 3.6$ cm coherent wave in proportion to their areas; particles in the Rayleigh regime remove energy as area cubed. For power-law size distributions with index greater than about -4 , the effects of particles less than about 1 cm in diameter can be neglected.
 9. A. L. Lane *et al.*, *Science* 215, 537 (1982).
 10. We thank V. R. Eshleman for several useful and illuminating discussions and our colleagues at Stanford, in particular R. A. Simpson, M. Plume, H. Zebker, F. Orabona, and L. W. Raley, for their efforts in reducing the ring occultation data. We thank the members of the Voyager Project, the members of the radio science team, and the members of the radio science support team at Jet Propulsion Laboratory for support during the planning, implementation, execution, and data acquisition phases of the experiment. This work was supported by the Planetary Atmospheres Program of the National Aeronautics and Space Administration and by Jet Propulsion Laboratory.

22 March 1982; revised 24 May 1982

Advection of Pore Fluids Through Sediments in the Equatorial East Pacific

Abstract. *Measurements of the ratio of helium-4 to helium-3 and of calcium ion in the pore waters of sediments at two locations in the eastern equatorial Pacific indicate that solution advection is occurring through the sediments. Both the helium ratio and the calcium ion profile yield velocity values for advective flow of about 20 centimeters per year. Mass balance constraints are also consistent with the interpretation presented. Flow appears to be occurring through relatively thick sediments, on the order of 300 meters.*

The subject of slow advective flow of solutions through marine sediments has received considerable attention over the past several years. Most discussions presented so far have been based upon interpretations of temperature profiles, with flow being determined from nonlinear temperature gradients in the absence of corresponding changes in thermal conductivity (1, 2). Advection consistent with thermal measurements also has been inferred from pore water Ca^{2+} profiles in relatively thin sediments (3). The case for advection in thick (> 100 m) sediments is, however, controversial, with chemical corroboration of flow based upon temperature profiles lacking. In the one case where chemical and

thermal data were collected simultaneously, discordant results were obtained, the chemical data (SO_4^{2-}) indicating little if any flow (4). In addition, velocities estimated from thermal data often are inconsistent with reasonable values of permeability, the hydrostatic head required to produce the estimated velocity being sufficient to "lift" the sediment overburden.

Characterization of the occurrence and nature of fluid flow through sediments is important from both a geochemical and a geophysical point of view. Such flow could provide a hitherto ignored conduit between the crust and the overlying ocean water, influencing heat transfer and the geochemical budgets of

many of the components of seawater. Recent papers (5) have drawn attention to high-temperature (350° to 400°C) interaction between seawater and basaltic crust and its chemical consequences. Substantial communication between much cooler crust and the ocean through sediments could markedly modify models of exchange based upon the high-temperature end-member.

At the velocities most commonly cited [1 to 50 cm year⁻¹ (1, 2)], chemical tracers should be better suited to measurement of flow than temperature. One available tracer is helium. Its diffusivity, "geochemistry," and precision of measurement make it ideally suited at reported advective velocities. Helium is effectively conservative in sediments, its production being slight (and correctable with uranium and thorium analyses) in the intervals sampled (0 to 10 m). Significant gradients are expected from uranium and thorium decay in the underlying

crust and sediments. In addition, since the isotopic ratio of this helium [⁴He/³He ≈ 10⁷ (6)] is distinctly different from that of seawater helium (⁴He/³He ≈ 10⁶), we expect an isotopic ratio anomaly that is, to a first order, independent of concentration variations in the "initial" helium content of the pore waters.

Samples for helium and Ca²⁺ analyses were collected at two sites in the eastern equatorial Pacific (7). Pore water solutions were collected by in situ means to avoid sampling artifacts. The procedures are similar to those described elsewhere (8) with two important modifications: the sample probes were emplaced hydraulically, permitting precise location relative to the interface (± 0.5 cm), and samples were drawn into titanium cylinders to prevent loss of helium. Solutions for helium analysis were expressed directly from the titanium cylinders into 0.8-ml aluminum tubing (0.3 cm outside diameter, 25 cm long), eliminating any expo-

sure to air. After the tubing was flushed with 5 to 8 ml of sample, it was sealed with pinch clamps. Solutions used for other analyses were stored in sealed polyethylene tubing.

The ⁴He/³He profiles are shown in Fig. 1a. The data are presented as a ratio to the air standard to reflect increases in ⁴He from uranium and thorium decay. All the samples were supersaturated with respect to both helium and neon, indicating a persistent and random inclusion of a small volume of air in the samples (< 0.01 cm³). We have corrected the data by normalizing the neon concentrations to equilibrium solubility and correcting the measured helium concentration and ⁴He/³He ratio by the indicated air contribution at atmospheric abundance ratios. Total helium profiles remain "noisy" as a result of a compounding of errors in a relatively large correction. The ⁴He/³He correction is "second order," however, and distributions in the pore waters are more reliably characterized by this variable than by total concentration. The fact that the shallowest samples correct to a value close to expected bottom-water isotopic ratios (0.78 *R_A*, where *R_A* is the atmospheric ⁴He/³He ratio), indicates that the corrections are appropriate and reliable.

Although scattered, the distribution of ⁴He/³He with depth is nonlinear. Input of ⁴He from within the sampled interval, given typical uranium and thorium contents (3 and 12 parts per million, respectively), could account for less than 0.1 percent of the observed curvature. Changes in diffusivity (Fig. 1c) cannot be responsible for the observed nonlinearity but rather contribute a curvature in the opposite sense. Only an upward flow of solution can produce the observed nonlinear distribution of ⁴He/³He.

Using an advection-diffusion model that incorporates depth-dependent diffusion, we find that the concentration of a conservative constituent, *C*, is given by

$$C_x = (C_0 - C_\infty) \exp\left(\int_0^x \frac{v}{D} dx\right) + C_\infty \quad (1)$$

where *C*₀ and *C*_{*x*} are the concentrations at depths *x* = 0 and *x*, respectively, *v* is the velocity of flow, and *D* is the effective bulk diffusion coefficient in the sediment. If we use resistivity (*R*) as an analog of diffusivity (*D*) (9), *D* can be represented reasonably well (Fig. 1c) by

$$\frac{D_{\text{sed}}}{D_{\text{sw}}} = \frac{R_{\text{sw}}}{R_{\text{sed}}} = a_1(1 - e^{-a_2x}) + a_3 \quad (2)$$

where *sed* and *sw* refer to sediment and seawater, respectively; *R* is resistivity; and *a*₁, *a*₂, and *a*₃ are the fitting constants. We can solve Eqs. 1 and 2 analytically.

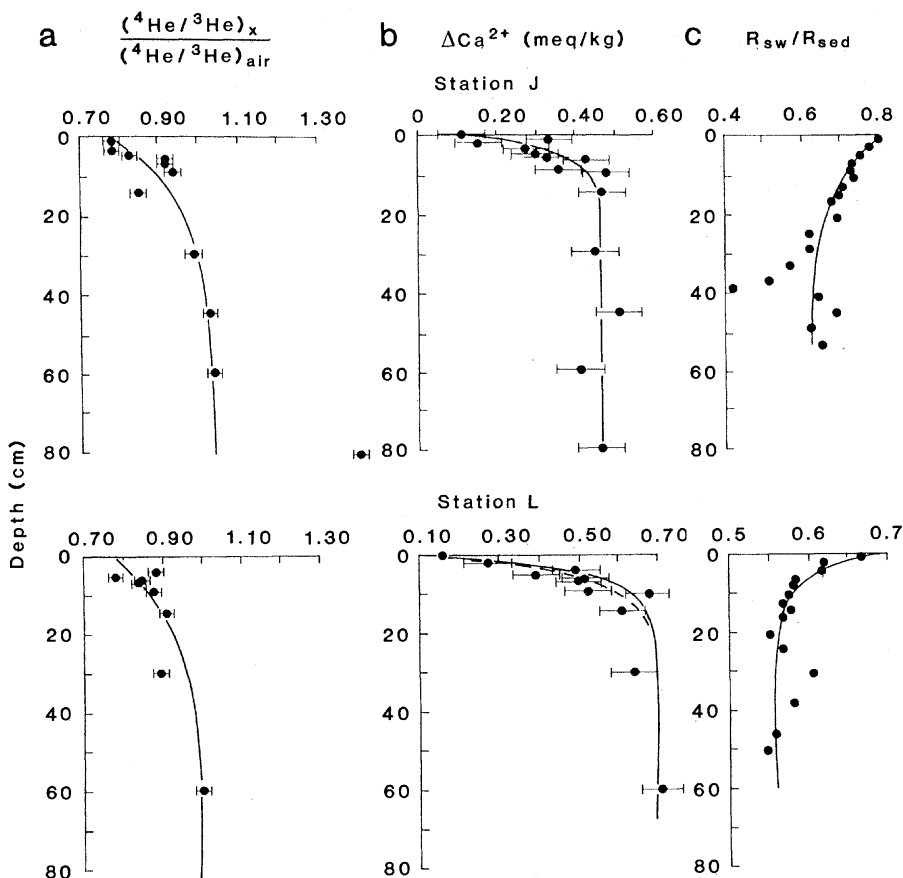


Fig. 1. (a) Distribution of ⁴He/³He with depth below the interface. The bottom-water value is that of Pacific bottom water, 0.78, and was not measured. The curve is the ratio predicted from Eq. 1. (b) Change in Ca²⁺ concentration with depth relative to bottom water. The curve is the predicted ΔCa²⁺ based upon the helium-determined velocity as given in the text and asymptotic (constant) ΔCa²⁺ at depth greater than 15 cm. The dashed curve for station L data is for a velocity of -12 cm year⁻¹; the solid curve for station L corresponds to a velocity of -16 cm year⁻¹. (c) Variation in sediment resistivity relative to that of bottom water with depth. The curves are the data fitted to Eq. 2 and used to define *D* as a function of depth. Data points from 33 to 49 cm (station J) have been omitted from the fit. The latter were measured in a coarse foram sand that was undersaturated as a result of the drainage of the pore water during sampling, yielding spuriously high *R*_{sed} values.

ically for constant v and regress the data for a best-fit value.

The fit of the $^4\text{He}/^3\text{He}$ data to the model is depicted in Fig. 2a, and the distribution predicted from it is indicated in Fig. 1a. The quantity (Fig. 2a) v is reasonably well constrained at station J, but the paucity of data below 15 cm leaves v poorly constrained at station L. The values obtained are -21 and -16 cm year^{-1} at stations J and L, respectively (negative = flow upward). The conservative profile of Ca^{2+} as ΔCa^{2+} , calculated from the well-constrained value of ΔCa^{2+} ($x > 15$ cm) and the helium-based v , is indicated in Fig. 1b along with the raw ΔCa^{2+} data. Within the uncertainty of the Ca^{2+} data, the profiles can be adequately explained as an essentially advective feature. No reaction in the upper 80 cm is required.

There is some evidence that the estimated value of v at station L is too large. The fit of the Ca^{2+} data to the predicted, conservative profile is improved if $v = -12$ cm year^{-1} . But Ca^{2+} is not conservative a priori, and deviation could reflect reaction. Should this be the case, however, the deviation could only be explained in terms of precipitation, quite contrary to the dissolution universally observed in deep-sea sediments (8; 10). Given the scatter in the data and the insensitivity of ΔCa^{2+} to velocity changes, the estimates cannot be considered to be more accurate than ± 5 cm year^{-1} .

It could be argued that the $^4\text{He}/^3\text{He}$ profiles are linear and hence purely diffusive. The data are scattered, and a straight line could be forced through the data if one ignored a few points. In this case $v = 0$ and the observed ΔCa^{2+} curvature is due to reaction in the upper 12 to 15 cm. A consideration of both Ca^{2+} and helium mass balances has direct bearing on the appropriateness of such an interpretation.

The Ca^{2+} mass balances for the sites studied argue against profiles controlled by diffusion and reaction. The sediments sampled at station J are CaCO_3 -free. Using conditions of sedimentation appropriate for this area, we estimate that solid Ca^{2+} accumulates at a rate of 0.7 mg cm^{-2} per 10^3 years (11). This input may be compared with an estimate of the diffusive loss of Ca^{2+} from within the sediment assuming a linear Ca^{2+} gradient between $x = 0$ and $x = 12$ cm, of 92 mg cm^{-2} per 10^3 years, some 100 times the input. With a wide margin for error, reaction alone could not supply the Ca^{2+} diffusing out of the sediments at steady state. A Ca^{2+} mass balance requires that virtually all the Ca^{2+} be supplied by advection, a conclusion consistent with

the fit of the ΔCa^{2+} data to the conservative advection profile (Figs. 1b and 2b).

The case for the necessity of advection at station L is only slightly weaker than at station J. The CaCO_3 content is nearly invariant at 72 percent. A conservative (linear) estimate of diffusive loss of Ca^{2+} from the sediments is 128 mg cm^{-2} per 10^3 years. Assuming noncarbonate accumulation as at station J yields a Ca^{2+} accumulation rate of ~ 100 mg cm^{-2} per 10^3 years. Thus the amount of Ca^{2+} advected downward through the 12-cm horizon by burial as CaCO_3 is about the same as that lost by upward diffusion through this same horizon. If reaction supplied the Ca^{2+} , all the CaCO_3 reaching 12 cm would be dissolved. This is not the case, as there is no discernible decrease in the percentage of CaCO_3 within the upper 30 cm at station L, and, as at station J, an advective source of Ca^{2+} is indicated.

The helium mass balances lead to similar conclusions. Estimating helium fluxes by assuming a linear gradient through the deepest data points yields conservative values of 1.6×10^5 $\text{atom cm}^{-2} \text{sec}^{-1}$ (station J) and 0.8×10^5 atom cm^{-2}

sec^{-1} (station L). Assuming an average sediment composition of 50 percent CaCO_3 as observed at Deep Sea Drilling Project site 83, supporting these fluxes would require sediment thicknesses of 1300 m (station J) and 650 m (station L). Sediment thicknesses in this area are reported to be only about 300 m (12). Support for the estimated fluxes would require diffusive communication with a vertical column of 300 m of sediment plus 10 to 20 km of basalt, the uranium and thorium content of the latter being only 3 percent that of sediment. This is possible but not likely, since some active means of ventilating this much crust would be required; advection provides a more viable alternative.

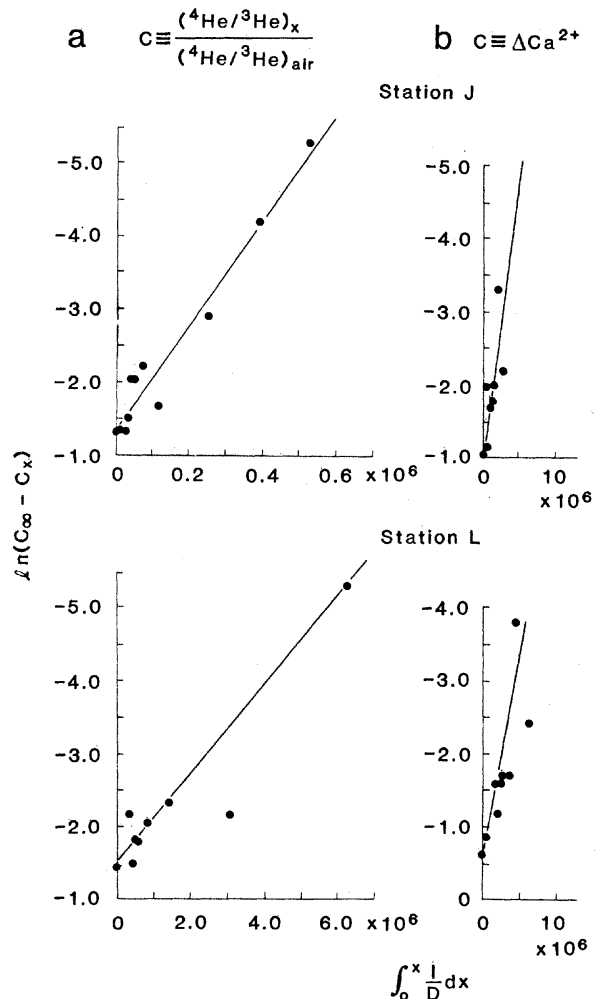
One caveat to our interpretation of the data should be noted. The models used assume a steady state. Should the distributions of both helium and Ca^{2+} be nonsteady state, then our mass balance calculations would be invalid. We cannot, however, test this possibility.

The occurrence of advection at these sites supports the contention that flow may occur through relatively thick sediment (13). Even though we have no seismic data, the sediments in this area

Fig. 2. Plots of Eq. 1 rearranged to the form

$$\ln(C_\infty - C_x) = v \int_0^x (1/D) dx + \ln(C_\infty - C_0)$$

(a) Values of $^4\text{He}/^3\text{He}$ plotted according to the above. The line is the least-squares fit of the data used to calculate v . (b) The ΔCa^{2+} data plotted according to the above. The line is the relationship predicted for ΔCa^{2+} from v as determined by the slope in (a) for conservative Ca^{2+} .



are reported to be on the order of 300 m thick (12). The data presented here suggest that, even where basement outcrops are absent, advective transport between the oceans and underlying basalt crust may occur.

The flow of water between basement and the oceans off ridge axes has considerable geochemical significance. Off ridge, the upper kilometer of basaltic crust is generally cool [$< 50^{\circ}\text{C}$ (14)]. The advective transport of heat under low-temperature conditions is unlikely to have the same heat-mass relations as those observed in the axial hot springs (5). Calculation of mass exchange by integration of total advective heat exchange for the oceans solely on the basis of the high-temperature (350° to 400°C) end-member must be incorrect. Should little reaction occur at low temperature, such estimates simply would be too high. If reaction between basalt and seawater occurs at low temperatures, as is likely, then the low-temperature reactions may run counter to the high-temperature ones, at least in some instances [for example, for K^+ , Li^+ , and possibly Mg^{2+} (15)], altering the overall flux estimates significantly.

FREDERICK L. SAYLES
WILLIAM J. JENKINS

Department of Chemistry,
Woods Hole Oceanographic Institution,
Woods Hole, Massachusetts 02543

References and Notes

- R. N. Anderson, M. A. Hobart, M. G. Langseth, *Science* **204**, 828 (1979); R. W. Embley, M. A. Hobart, R. N. Anderson, *Eos* **60**, 383 (1979).
- R. P. von Herzen, J. Crowe, K. Green, *Eos* **60**, 382 (1979).
- C. Maris and M. Bender, *ibid.* **61**, 995 (1980).
- J. Crowe and R. E. McDuff, *Earth Planet. Sci. Lett.*, in press.
- J. M. Edmond, C. Measures, R. E. McDuff, L. H. Chan, B. Grant, L. I. Gordon, J. B. Corliss, *ibid.* **46**, 1 (1979).
- P. Morrison and J. Pine, *Ann. N.Y. Acad. Sci.* **62**, 69 (1955).
- At station J ($7^{\circ}03.2'N$, $91^{\circ}42.5'W$), the water depth is 3561 m; sediments are pelagic clay (0 percent CaCO_3). At station L ($4^{\circ}30.8'N$, $91^{\circ}52.8'W$) the water depth is 3112 m; sediments are clayey carbonate (72 percent CaCO_3).
- F. L. Sayles, P. C. Mangelsdorf, Jr., T. R. S. Wilson, D. N. Hume, *Deep-Sea Res.* **23**, 259 (1976); F. L. Sayles, *Geochim. Cosmochim. Acta* **43**, 527 (1979).
- F. T. Manheim and L. S. Waterman, *Init. Rep. Deep Sea Drill. Proj.* **22**, 663 (1974); R. E. McDuff and J. M. Gieskes, *Earth Planet. Sci. Lett.* **33**, 1 (1976).
- F. L. Sayles, *Geochim. Cosmochim. Acta* **45**, 1061 (1981).
- Estimation of Ca^{2+} accumulation is based on the measured parameters porosity (ϕ) = 0.90, grain density = 2.8 g cm^{-3} , an assumed Ca^{2+} content = 0.86 percent (by weight) [S. Landergrén, *Rep. Swed. Deep-Sea Exped. 1947-1948*, **10**, 57 (1964)], and a sedimentation rate = 0.3 cm per 10^3 years measured at the nearby Manganese Nodule Project site H. The latter is consistent with the values of 0.1 to 0.5 cm per 10^3 years reported for this area [T.-L. Ku, W. S. Broecker, N. Oepdyke, *Earth Planet. Sci. Lett.* **4**, 1 (1968)].
- W. J. Ludwig and R. Houtz, *Isopach Map of the East Pacific*, American Association of Petroleum Geologists Map Series (1979); Tj. H. van Andel *et al.*, *Geol. Soc. Am. Bull.* **82**, 1489 (1971).

- Von Herzen *et al.* (2) noted that in the region where they postulated the existence of fluid flow the sediments are "at least several hundred meters" thick.
- R. N. Anderson, M. G. Langseth, J. G. Sclater, *J. Geophys. Res.* **82**, 3391 (1977).
- Edmond *et al.* (5) reported the enrichment of K^+ and Li^+ and the depletion of Mg^{2+} in hydrothermal solutions. G. Thompson [*Eos* **54**, 1015 (1973)] has demonstrated the uptake of K^+ and Li^+ in basalts during low-temperature alteration.

- We are grateful to P. Mangelsdorf, Jr., S. Emerson, M. Bender, and F. T. Manheim for their helpful criticisms of the manuscript. Many of the $^4\text{He}/^3\text{He}$ analyses were done by T. Torgerson. Sampling was done with the aid of the officers and crew of the R.V. *Knorr*, in particular, J. Cotter. Financial support has been provided by NSF grants OCE 78-24685, OCE 79-19023, and EAR 77-23170. This is Woods Hole Oceanographic Institution Contribution No. 5076.

3 August 1981; revised 13 April 1982

The Anticancer Agent Adriamycin Can Be Actively Cytotoxic Without Entering Cells

Abstract. *The antineoplastic agent adriamycin was coupled to an insoluble agarose support. This material was actively cytotoxic to L1210 cells in culture under conditions in which no free adriamycin could enter the cell. It is concluded that an agent whose principal target was previously thought to be DNA can exert its cytotoxic action solely by interaction at the cell surface.*

Adriamycin is one of the most important agents used in the treatment of human cancer. Historically, DNA has been considered to be the primary target for the cytotoxic action of this drug on susceptible cells (1). The DNA receptor hypothesis is attractive on structural

grounds because adriamycin does bind, with reasonably high affinity, double-stranded nucleic acids by intercalation (2, 3) and because drug fluorescence accumulates in the nuclei of treated cells (4).

There are reasons, however, to question whether DNA interaction is a sufficient explanation for the ability of adriamycin to kill tumor (or any) cells. For example, if one reviews the literature on the hundreds of anthracycline derivatives synthesized, no obvious relation emerges between the ability to inhibit nucleic acid synthesis and cytotoxicity. Moreover, anthracycline synthesis programs in various laboratories have produced active adriamycin-like drugs that have no demonstrable ability to bind DNA, effectively ruling out DNA intercalation as an absolute requirement in cytotoxic action. For example, *N*-trifluoroacetyl adriamycin-14-valerate is an active anthracycline with little or no ability to bind DNA (5). Even the effects of the single agent adriamycin on cell viability are not tightly coupled to inhibition of DNA or RNA synthesis (6).

Many membrane activities are modulated by adriamycin, including lectin interaction (7), glycoprotein synthesis (8), phospholipid structure and organization (9), fluidity (10), fusion properties (11), transport of small molecules and ions (12), and expression of hormone receptors (13). The anthracyclines can act on biological membranes, but this does not necessarily mean that their cytotoxic effects on cancer cells are mediated by membrane interactions.

In this report we present evidence that the cell surface is a target for the action of adriamycin. Our approach was to expose murine cancer cells (line L1210) to large, insoluble, polymeric beads to

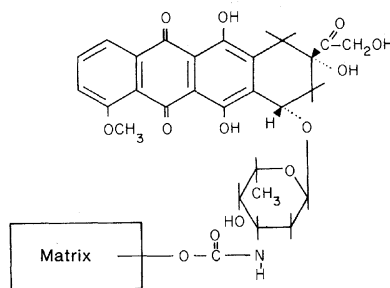


Fig. 1. Structure of adriamycin linked to a polymeric matrix. The activated polymer (Reacti-gel 6x, Pierce Chemical) consists of 6 percent cross-linked agarose beads (40 to 210 μm in diameter) derivatized with 1,1'-carbonyldiimidazole, which can react with free amino groups. In a typical synthesis 1×10^{-8} to 2×10^{-8} mole of adriamycin is allowed to react per milligram of activated agarose (molar ratio of imidazolyl carbamate to adriamycin is about 12:1). The synthesis is carried out for 24 to 72 hours in 0.1M borate buffer at pH 8.0 and 4°C . Under these conditions 20 to 40 percent of the adriamycin becomes covalently attached to the beads; the remaining unreacted imidazole carbamate groups are eliminated with an excess of hydroxylamine. Unattached adriamycin is removed by exhaustive washing (2 weeks of continuous exposure) with borate buffer, acetonitrile, and methanol. Large volumes (0.5 to 1 liter) from the washings are collected, evaporated under reduced pressure, and assayed for adriamycin by high-pressure liquid chromatography (14). These washings do not damage the structural integrity of the beads, as judged by light microscopy. The washings are continued until no free drug can be detected. The resulting immobilized adriamycin is stored in the dark at 4°C . It does not release free drug for at least several months.